

TEFormer: Texture-Aware and Edge-Guided Transformer for Semantic Segmentation of Urban Remote Sensing Images

Guoyu Zhou, Jing Zhang, *Member, IEEE*, Yi Yan, Hui Zhang, *Member, IEEE*, and Li Zhuo, *Member, IEEE*

Abstract—Semantic segmentation of urban remote sensing images (URSI) is crucial for applications such as urban planning and environmental monitoring. However, geospatial objects often exhibit subtle texture differences and similar spatial structures, which can easily lead to semantic ambiguity and misclassification. Moreover, challenges such as irregular object shapes, blurred boundaries, and overlapping spatial distributions of semantic objects contribute to complex and diverse edge morphologies, further complicating accurate segmentation. To tackle these issues, we propose a texture-aware and edge-guided Transformer (TEFormer) that integrates texture awareness and edge-guidance mechanisms for semantic segmentation of URSIs. In the encoder, a texture-aware module (TaM) is designed to capture fine-grained texture differences between visually similar categories to enhance semantic discrimination. Then, an edge-guided tri-branch decoder (Eg3Head) is constructed to preserve local edges and details for multiscale context-awareness. Finally, an edge-guided feature fusion module (EgFFM) is to fuse contextual and detail information with edge information to realize refined semantic segmentation. Extensive experiments show that TEFormer achieves mIoU of 88.57%, 81.46%, and 53.55% on the Potsdam, Vaihingen, and LoveDA datasets, respectively, shows the effectiveness in URSI semantic segmentation.

Index Terms—urban remote sensing images, semantic segmentation, texture-aware, edge guidance, feature fusion

I. INTRODUCTION

SEMANtic segmentation of urban remote sensing images (URSI) involves assigning semantic labels to individual pixels based on image content, such as buildings, vehicles, and trees [1]. This task is fundamental to various applications, including urban planning, environmental monitoring, and disaster response. Compared with general RSI, URSI is characterized by densely distributed objects, complex spatial structures, and a wide range of object scales. These characteristics introduce higher accuracy demands and pose significant challenges for semantic modeling.

Current mainstream segmentation methods can be broadly categorized into convolutional neural network (CNN)-based and Transformer-based approaches. CNNs have been widely

employed in early RSI semantic segmentation task due to their robust capability in extracting local features. Ronneberger *et al.* [2] introduced skip connections to mitigate detail loss during downsampling. Li *et al.* [3] proposed a lightweight pure convolutional module that captures both global context and local textures. However, CNNs inherently struggle to model long-range dependencies and complex spatial relationships due to their limited receptive fields. Transformer-based architectures have recently gained traction for the ability to capture global context. Nevertheless, challenges persist in handling complex category distributions and blurred object boundaries commonly found in RSI. To address these limitations, several enhancements have been proposed. Wang *et al.* [4] designed a global-local attention mechanism in the decoder. Fan *et al.* [5] introduced a detail-structure preservation module to mitigate the loss of detail and structure information. Wu *et al.* [6] leveraged the spatial-specific Transformer with involution for semantic segmentation. Ma *et al.* [7] fused CNN with Transformer to compensate for their respective weaknesses. These works highlight the potential of combining local structural modeling with global contextual reasoning for improved segmentation. For example, our previous work D²SFormer [8] integrated cross-shaped window self-attention with convolutional channel attention to effectively capture both global and local features, achieving improved segmentation performance on URSIs. However, it lacks to explicitly model texture or boundary information, leaving room for further enhancement.

In URSI, since objects with similar spatial layouts often differ in texture and edge feature, such fine-grained details are critical for accurate segmentation. Texture features describe surface properties—such as roughness and regularity—and are often extracted via wavelet transforms or frequency-domain analysis. Previous studies, including the texture enhancement attention module [9] and the quantization and counting operator (QCO) [10], have shown that leveraging texture can significantly improve category discrimination. Notably, the dual-path network proposed by Li *et al.* [3], which jointly

This work was supported in part by the Beijing Natural Science Foundation under Grant L247025. (Corresponding author: Jing Zhang, Hui Zhang).

All authors are with the School of Information Science and Technology, Beijing University of Technology, Beijing 100124, China, and Jing Zhang, Li Zhuo are also with the Beijing Key Laboratory of Computational Intelligence and Intelligent System, Beijing University of Technology, Beijing 100124, China (e-mail: zhouguoyu@emails.bjut.edu.cn; zhj@bjut.edu.cn; yany1581@163.com; huizhang@bjut.edu.cn; zhuoli@bjut.edu.cn).

This work has been submitted to the IEEE for possible publication. Copyright may be transferred without notice, after which this version may no longer be accessible.

models contextual information and local texture information, offers valuable insights for our design. On the other hand, edge features provide contour information crucial for boundary localization. Techniques such as dynamic hybrid gradient convolution [11], three-branch architectures [12], and active boundary loss [13] have proven effective in improving edge prediction. In URSIs, boundary pixels often lie at interfaces between semantic classes and are prone to misclassification. Thus, precise extraction of edge features is essential for improving segmentation accuracy.

Some geospatial objects in URSI exhibit similar spatial shapes but possess subtle differences in texture, which can serve as key cues for distinguishing them. To this end, we propose a texture-aware and edge-guided Transformer (TEFormer). In the encoder, we use the texture-aware module (TaM) to perceive textural differences among similar objects and to mine fine-grained texture features. Meanwhile, the frequent occurrence and co-occurrence of irregular shapes, blurred boundaries, and overlapping spatial distributions among semantic objects result in highly complex and diverse edge morphologies at the pixel level. To handle this, we propose an edge-guided tri-branch decoder (Eg3Head), comprising ① the edge branch, which preserves original image edges; ② the detail branch, which employs a detail analysis module (DAM) [12] to extract fine semantic features; and ③ the context branch, which uses a parallel aggregation spatial pyramid pooling module (PASPPM) to aggregate multi-scale contextual information under a large receptive field. Finally, the edge-guided feature fusion module (EgFFM) is introduced to effectively integrate edge information into the learning of semantic features. This allows the model to trust detail information more around boundary regions while utilizing contextual information to fill the interiors of targets, thereby improving both overall semantic segmentation accuracy and edge refinement. The main contributions of this work are summarized as follows:

- We integrate texture awareness and edge-guided mechanisms to jointly model local texture and global contextual features, so as to improve the ability to distinguish between objects with similar spatial structures.
- TaM is introduced to enable fine-grained texture modeling, thereby enhancing sensitivity to low-level texture variations while improving semantic discrimination capability.
- An edge-guided three-branch structure, PASPPM, and EgFFM are combined to capture boundary detail and contextual information to guide multi-feature fusion for accurate URSI semantic segmentation.

II. METHODOLOGY

A. Overall

Our TEFormer comprises two core components: a texture-aware Transformer encoder and edge-guided three-branch decoder, as illustrated in **Fig. 1**. The encoder includes four feature extraction stages: TaM is embedded in Stages 1, 2 to enhance low-level texture features, while Stages 3, 4 employ the dual attention Transformer encoder from our previously proposed D²SFormer [8] for capturing rich global and local information. The texture-aware block integrates TaM, cross-shaped window self-attention (CWSA), and convolutional channel attention block (CCAB) [8] in parallel, improving sensitivity to subtle texture differences. The decoder consists of edge, detail, and context branches. Features $E_1 \sim E_4$ are processed through the edge and detail branches to extract P_e , P_{d1} , and P_{d2} , respectively, while E_4 is fed into the context branch to obtain P_c . Subsequently, P_e , P_{d2} , and P_c are fused using the EgFFM, and further combined with E_1 to generate the integrated feature G . Finally, G is passed through an MLP followed by a softmax function to perform semantic segmentation. Notably, dynamic upsampling is adopted to better recover object boundaries and reduce artifacts.

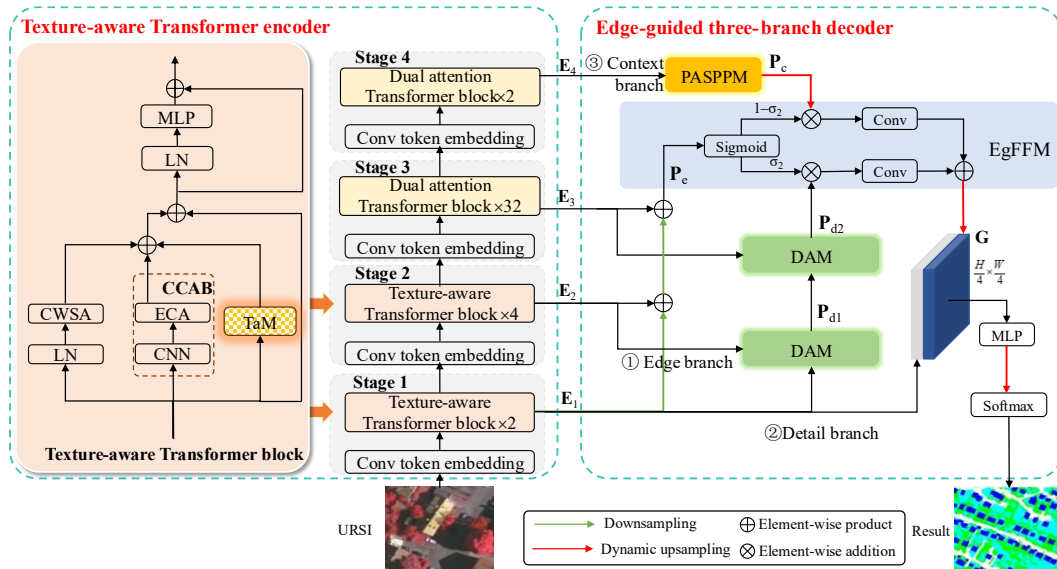


Fig. 1. The overall architecture of TEFormer.

B. Texture-Aware Module

Due to the complex textures and continuously distributed spectral features in URSI, conventional convolutions struggle to model global statistical textures despite their strength in capturing local edges. Inspired by the concept of histogram equalization, we introduce a QCO that constructs a texture descriptor by performing cosine similarity computation, quantization, counting, and feature encoding. This approach enhances global statistical texture modeling with low computational overhead. Specifically, the input features are discretized into L quantization levels, and quantized counting features are generated by counting and encoding each level.

However, directly fusing QCO features may result in spatial misalignment or low-order degradation. To address this, we design the TaM, which integrates QCO with an attention mechanism to focus on texture-similar regions. In addition, a multi-scale QCO is employed to reassign quantization levels, further enhancing texture contrast. The structure of TaM is illustrated in Fig. 2.

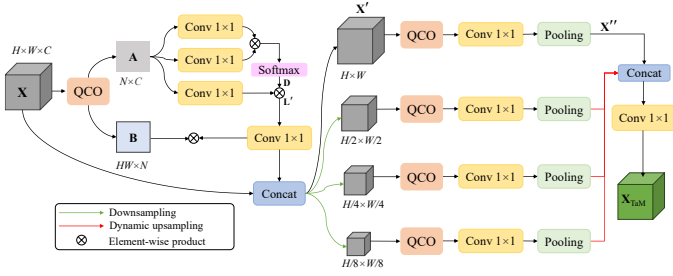


Fig. 2. The structure of TaM.

Given the input feature $\mathbf{X} \in \mathbb{R}^{H \times W \times C}$, the module proceeds as follows:

- (1) The QCO is applied to quantify the feature distribution, producing the quantized counting feature $\mathbf{A} \in \mathbb{R}^{N \times C}$ and an N -level quantization encoding matrix $\mathbf{B} \in \mathbb{R}^{HW \times N}$.
- (2) A graph adjacency matrix $\mathbf{D} \in \mathbb{R}^{N \times N}$ is constructed following the attention mechanism to update the quantization levels $\mathbf{L}' \in \mathbb{R}^{N \times C}$.

$$\mathbf{L}' = \text{Conv}(\mathbf{A}) \cdot \text{Softmax}(\text{Conv}(\mathbf{A})^T \cdot \text{Conv}(\mathbf{A})). \quad (1)$$

- (3) After combining \mathbf{L}' with \mathbf{B} , they are concatenated with \mathbf{X} to generate the enhanced feature \mathbf{X}' .

$$\mathbf{X}' = \text{Concat}(\text{Conv}(\mathbf{L}') \cdot \mathbf{B}, \mathbf{X}). \quad (2)$$

- (4) The feature \mathbf{X}' is processed through four branches at different scales. In each branch, the QCO is applied again to extract multi-scale texture features, followed by Conv and Pool to capture more abstract semantic information \mathbf{X}'' :

$$\mathbf{X}'' = \text{Pool}(\text{Conv}(\text{QCO}(\mathbf{X}'))). \quad (3)$$

- (5) The features from all four scales are dynamically upsampled and concatenated to fuse into the texture features \mathbf{X}_{TaM} .

$$\mathbf{X}_{\text{TaM}} = \text{Conv}(\text{Concat}(\text{dys}(\mathbf{X}''_{1/8}), \text{dys}(\mathbf{X}''_{1/4}), \text{dys}(\mathbf{X}''_{1/2}), \mathbf{X}'')) \quad (4)$$

C. Edge-Guided Three-Branch Decoder

To obtain more comprehensive feature representations, we propose a lightweight Eg3Head, which comprises an edge branch, a detail branch, and a context branch.

The edge branch is to retain more complete and detailed object boundaries. Multi-level features extracted by the encoder are first downsampled and summed sequentially to generate the edge feature map \mathbf{P}_e . In the detail branch, DAM is introduced to selectively learn semantic representations from features \mathbf{E}_1 to \mathbf{E}_3 , thereby preserving more local structural information. The context branch employs PASPPM to aggregate multi-scale contextual features. This module combines long-range dependencies modeled via average pooling with the large receptive field of dilated convolutions, effectively representing features at spatial scales. Residual connections are used within PASPPM to balance new feature learning with the preservation of original information. The detailed structure of PASPPM is shown in Fig. 3(a).

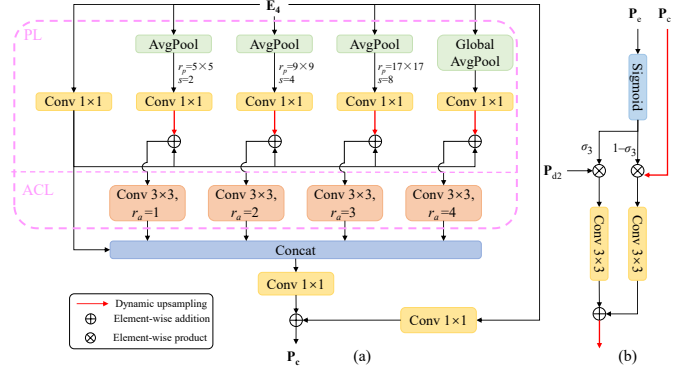


Fig. 3. The structure of PASPPM and EgFFM.

D. Edge-Guided Feature Fusion Module

The context branch provides richer semantic representations but often loses spatial details. In contrast, the detail branch retains edge and texture information but lacks high-level semantic guidance and is prone to artifacts. To effectively combine their strengths, we design the EgFFM, as illustrated in Fig. 3(b). EgFFM leverages boundary information to adaptively regulate the contribution of each branch, enabling more balanced and flexible feature fusion.

A sigmoid operation is applied to \mathbf{P}_e to produce a weight score σ_3 , and the fusion process is formulated as:

$$\mathbf{F}_{\text{EgFFM}} = \text{dys}(\text{Conv}(\sigma_3 \cdot \mathbf{P}_{d2}) + \text{Conv}((1 - \sigma_3) \cdot \text{dys}(\mathbf{P}_e))) \quad (5)$$

When $\sigma_3 > 0.5$, more trust is placed on detail features; otherwise, context features dominate. This dynamic weighting mechanism allows EgFFM to adaptively balance the contributions of different branches, improving integration and segmentation performance on URSI.

III. EXPERIMENTS

A. Dataset

We evaluate the performance of our TEFormer on the ISPRS Potsdam/Vaihingen dataset [14], and the LoveDA dataset [15]. These datasets contain diverse urban object categories (e.g., car

>GRSL-01930-2025<

and building) and are widely utilized for semantic segmentation in URSIs. Specifically, for the LoveDA dataset, we perform a focused evaluation on five major urban categories: background, building, road, water, and barren.

1) **Potsdam** dataset contains 38 samples with a resolution of 6000×6000 pixels. It includes six land cover classes: impervious surface, tree, building, low vegetation, car, and background. In our experiments, the dataset was randomly split into training, validation, and test sets at a ratio of 7:1:2.

2) **Vaihingen** dataset consists of 33 samples with an average size of 2494×2064 pixels, including near-infrared (NIR), red (R), and green (G) bands. It shares the same categories as Potsdam. Similar to Potsdam, the dataset was randomly divided into training, validation, and test sets at a ratio of 7:1:2.

3) **LoveDA** dataset includes 5,987 high-resolution remote sensing images, each sized 1024×1024 pixels. It contains seven land cover classes: background, building, road, water, barren, forest, and agriculture. Following the official split, we used 2,522 images for training, 1,669 for validation, and 1,796 for testing.

B. Implementation Details

Experiments were conducted in PyTorch on a TITAN Xp GPU, training for 160k iterations with AdamW (lr=6e-5, weight decay=0.01, batch size=2) on 512×512 image patches. For evaluation, we adopted mean Intersection over Union (mIoU), mean F1 score (mF1), and pixel accuracy (PA). Model complexity was measured in terms of parameter count (Params), floating-point operations per second (FLOPs), and test time.

C. Comparison with Other Methods

To evaluate our method, we conducted comparisons with several mainstream semantic segmentation methods (see **Table I**) including BiFormer [16], CMTFNet [17], Spatial-specificT [6], ESST [18], TransNeXt [19], and our prior -D²SFormer [8], all of which are available on a TITAN Xp GPU.

1) **Potsdam**: TEFormer achieves the best performance, with an

mIoU of 88.57%, mF1 of 94.37%, PA of 94.98%. Compared to D²SFormer, TEFormer yields an mIoU improvement of 0.73%. These gains are attributed to the integration of TaM in the encoder and Eg3Head, which together enhance the model's ability to capture subtle texture variations and leverage edge cues to guide the fusion of contextual and detailed features. Compared to other methods, TEFormer also benefits from PASPPM's large receptive field for effective multi-scale context aggregation. **Fig. 4** (Line 1) illustrates some qualitative results on the Potsdam dataset. TEFormer demonstrates superior category discrimination and boundary delineation, validating the effectiveness of its texture-aware and edge-guided design.

2) **Vaihingen**: TEFormer reaches the best results across multiple key metrics, including 81.46% mIoU, 89.24% mF1, and 90.64% PA. Its texture-aware encoder enhances discrimination of similar geospatial objects, while the Eg3Head effectively fuses contextual, detailed, and edge features for accurate segmentation. Compared to other models, TEFormer achieves notably better results. As shown in **Fig. 4** (Line 2), TEFormer delivers more precise boundaries and improved segmentation in complex scenes, particularly where textures are similar or regions are interleaved.

3) **LoveDA**: While its mIoU is slightly below BiFormer, TEFormer notably outperforms D²SFormer and achieves competitive results, particularly in building and road categories, reflecting stronger land cover recognition. This improvement stems from its edge-guided design, which enhances boundary modeling and reduces local ambiguity. As illustrated in **Fig. 4** (Line 3), TEFormer achieves more accurate and complete segmentation, particularly in class distinction.

4) **Complexity analysis**: although TEFormer exhibits higher complexity than CMTFNet and D²SFormer due to its texture-aware and edge-guided modules, with 52.67M Params, 72.25G FLOPs, and a test time of 0.101s, it achieves the highest segmentation accuracy. These results indicate that TEFormer maintains a favorable balance between performance and efficiency.

TABLE I
COMPARISON WITH THE SOTA METHODS ON THREE DATASETS

Method	Potsdam			Vaihingen			LoveDA						Params (M)	FLOPs (G)	Test time (s)
	mIoU (%)	mF1 (%)	PA (%)	mIoU (%)	mF1 (%)	PA (%)	Back- ground	Build- ing	Road	Water	Barren	mIoU (%)			
BiFormer [16]	85.28	92.89	93.34	80.93	88.89	90.36	46.3	<u>60.0</u>	61.02	81.02	19.44	53.74	55.22	231.27	0.109
CMTFNet [17]	83.57	90.93	90.77	77.95	87.42	89.24	37.27	45.95	47.61	69.92	12.14	44.13	<u>30.07</u>	32.85	0.075
Spatial-specificT [6]	87.61	93.26	93.97	80.08	88.74	90.36	46.05	57.31	58.41	79.47	16.05	51.81	58.96	81.91	0.196
ESST [18]	87.81	93.43	93.94	79.36	88.27	90.06	42.3	48.86	51.44	75.56	11.88	47.07	28.01	60.67	<u>0.088</u>
TransNeXt [19]	87.22	93.76	94.28	81.14	88.82	90.47	33.42	60.4	57.56	79.88	14.95	50.32	58.41	238.68	0.144
D ² SFormer [8]	<u>87.84</u>	<u>94.02</u>	<u>94.63</u>	<u>81.24</u>	<u>88.99</u>	<u>90.55</u>	<u>46.97</u>	59.09	59.35	80.54	<u>19.45</u>	53.19	52.10	<u>51.42</u>	0.094
TEFormer(ours)	88.57	94.37	94.98	81.46	89.24	90.64	47.2	<u>60.0</u>	<u>60.07</u>	<u>80.87</u>	19.54	<u>53.55</u>	52.67	72.25	0.101

Note: Bold indicates the best, and underlined indicates the second best.

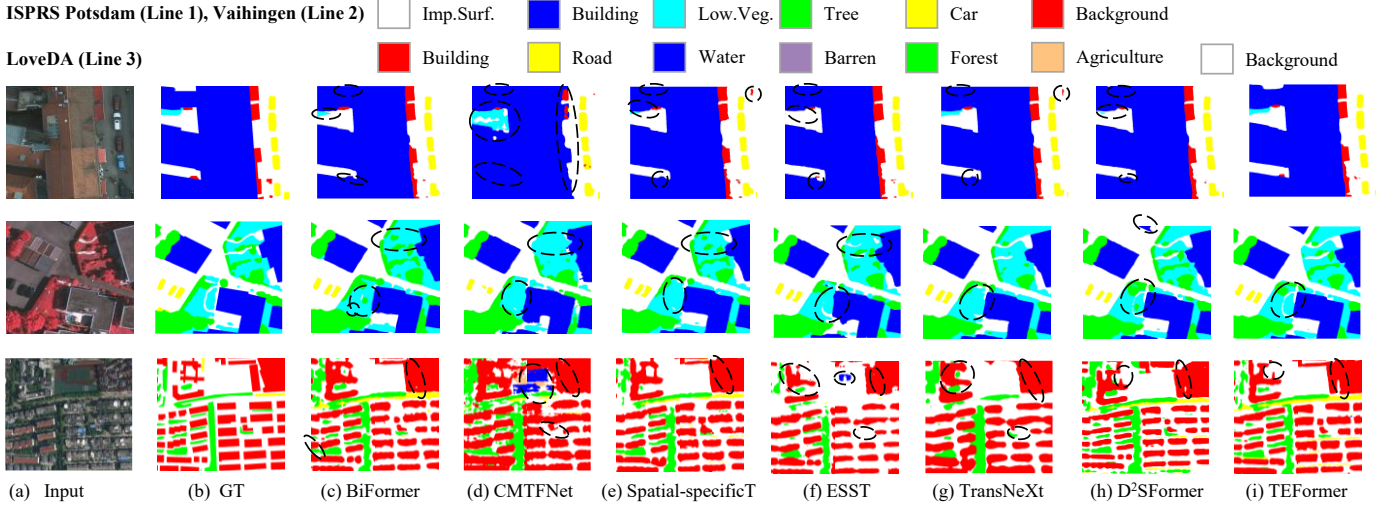


Fig. 4. Some examples of qualitative results.

D. Ablation Studies

To demonstrate the effectiveness of the proposed method, ablation studies were conducted on the Potsdam dataset focusing on the TaM and the Eg3Head components.

1) *Effectiveness of the TaM*: The TaM enhances the texture detail representation of low-level features by incorporating the QCO and dynamically adjusting the quantization levels. To evaluate its effectiveness, ablation experiments were conducted using the same decoder. Results (Fig. 5) show that while the introduction of QCO alone slightly degrades performance, the full TaM significantly improves performance by better focusing on critical texture information.

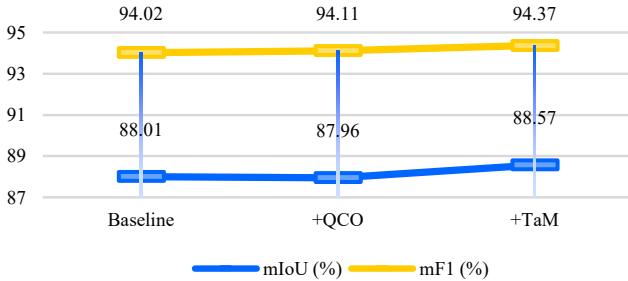


Fig. 5. Effectiveness of the TaM.

2) *Effectiveness of the Eg3Head*: To validate the decoder design, ablation experiments were conducted on the Potsdam dataset. As shown in Table II, the progressive integration of PASPPM, DAM, and EgFFM leads to consistent performance gains, confirming their effectiveness in feature extraction and fusion. These results highlight the decoder's capability in addressing the complexity of URSI semantic segmentation.

Group	PASPPM	DAM	EgFFM	mIoU (%)
1	—	—	—	87.21
2	✓	—	—	87.82
3	—	✓	—	87.78
4	✓	✓	—	88.20
5	✓	✓	✓	88.57

IV. CONCLUSION

To address the challenges of texture similarity and blurred boundaries in URSI semantic segmentation, we propose TEFormer that integrates texture-aware and edge-guided mechanisms to enhance regional discriminability and boundary representation by leveraging texture features, edge-guided decoding, and multi-scale fusion. The results outperform some comparative methods across multiple datasets, with a competitive in detail and edge segmentation. For future work, we will explore lightweight model designs and multi-source data integration to further improve generalization capability.

REFERENCES

- [1] Z. Xu, C. Su, and X. Zhang, "A semantic segmentation method with category boundary for land use and land cover (LULC) mapping of very-high resolution (VHR) remote sensing image," *Int. J. Remote Sens.*, vol. 42, no. 8, pp. 3146-3165, 2021.
- [2] O. Ronneberger, P. Fischer, and T. Brox, "U-Net: Convolutional networks for biomedical image segmentation," in *Proc. Med. Image Comput. Comput.-Assist. Intervention*, 2015: Springer, pp. 234-241.
- [3] B. Li, Y. Zhang, Y. Zhang, B. Li, and Z. Li, "Dual-path feature fusion network for semantic segmentation of remote sensing images," *IEEE Geosci. Remote Sens. Lett.*, vol. 21, pp. 1-5, 2024.
- [4] L. Wang *et al.*, "UNetFormer: A UNet-like Transformer for efficient semantic segmentation of remote sensing urban scene imagery," *ISPRS J. Photogramm. Remote Sens.*, vol. 190, pp. 196-214, 2022.
- [5] L. Fan, Y. Zhou, H. Liu, Y. Li, and D. Cao, "Combining Swin Transformer with UNet for remote sensing image semantic segmentation," *IEEE Trans. Geosci. Remote Sens.*, vol. 61, pp. 1-11, 2023.
- [6] X. Wu, J. Zhang, W. Li, J. Li, L. Zhuo, and J. Zhang, "Spatial-specific Transformer with involution for semantic segmentation of high-resolution remote sensing images," *Int. J. Remote Sens.*, vol. 44, no. 4, pp. 1280-1307, 2023.
- [7] Y. Ma, Y. Wang, X. Liu, and H. Wang, "SWINT-RESNet: An improved remote sensing image segmentation model based on Transformer," *IEEE Geosci. Remote Sens. Lett.*, 2024.
- [8] Y. Yan, J. Li, J. Zhang, L. Wang, and L. Zhuo, "D²SFormer: Dual attention-dynamic bidirectional Transformer for semantic segmentation of urban remote sensing images," *IEEE J. Sel. Top. Appl. Earth Observ. Remote Sens.*, vol. 18, pp. 12248-12262, 2025.
- [9] Z. Wan, Q. Zhang, and G. Zhang, "Low-level feature enhancement network for semantic segmentation of buildings," *IEEE Geosci. Remote Sens. Lett.*, vol. 19, pp. 1-5, 2022.
- [10] L. Zhu, D. Ji, S. Zhu, W. Gan, W. Wu, and J. Yan, "Learning statistical texture for semantic segmentation," in *Proc. IEEE Conf. Comput. Vis. Pattern Recognit. (CVPR)*, 2021, pp. 12537-12546.

- [11] J. Hou, Z. Guo, Y. Wu, W. Diao, and T. Xu, "BSNet: Dynamic hybrid gradient convolution based boundary-sensitive network for remote sensing image segmentation," *IEEE Trans. Geosci. Remote Sens.*, vol. 60, pp. 1-22, 2022.
- [12] J. Xu, Z. Xiong, and S. P. Bhattacharyya, "PIDNet: A real-time semantic segmentation network inspired by PID controllers," in *Proc. IEEE Conf. Comput. Vis. Pattern Recognit. (CVPR)*, 2023, pp. 19529-19539.
- [13] C. Wang *et al.*, "Active boundary loss for semantic segmentation," in *Proc. AAAI Conf. Artif. Intell.*, 2022, vol. 36, pp. 2397-2405.
- [14] "ISPRS 2d semantic labeling contest," ISPRS Working Group, 2021.
- [15] J. Wang, Z. Zheng, A. Ma, X. Lu, and Y. Zhong, "LoveDA: A remote sensing land-cover dataset for domain adaptive semantic segmentation," in *Proc. Adv. Neural Inf. Process. Syst.*, Dec. 2021, pp. 1-12.
- [16] L. Zhu, X. Wang, Z. Ke, W. Zhang, and R. Lau, "BiFormer: Vision Transformer with bi-level routing attention," in *Proc. IEEE Conf. Comput. Vis. Pattern Recognit. (CVPR)*, 2023, pp. 10323-10333.
- [17] H. Wu, P. Huang, M. Zhang, W. Tang, and X. Yu, "CMTFNet: CNN and multiscale Transformer fusion network for remote-sensing image semantic segmentation," *IEEE Trans. Geosci. Remote Sens.*, vol. 61, 2023, Art no. 2004612.
- [18] Y. Yan, J. Zhang, X. Wu, J. Li, and L. Zhuo, "When zero-padding position encoding encounters linear space reduction attention: an efficient semantic segmentation Transformer of remote sensing images," *Int. J. Remote Sens.*, vol. 45, no. 2, pp. 609-633, 2024.
- [19] D. Shi, "TransNeXt: Robust foveal visual perception for vision Transformers," in *Proc. IEEE Conf. Comput. Vis. Pattern Recognit. (CVPR)*, 2024, pp. 17773-17783.